780307

The Oscillations of a Flexible Castor, and the Effect of Front Fork Flexibility on the Stability of Motorcycles

G. E. Roe
Simon Engrg. Lab.
Univ. of Manchester (England)
W. M. Pickering and A. Zinober
Dept. of Applied Maths and Computing Science
Univ. of Sheffield (England)

ANY STEERED ROLLING WHEEL whose contact patch with the ground lies behind the intersection of the steering axis with the ground can be termed a castor, and the steering oscillations of such castors are well known but little understood in many applications. These oscillations range from the 'shimmy' of the simple tea-trolley wheel, to the wobble of aircraft landing wheels and the weaving of towed vehicles and trailers. It is paradoxical that the trailing contact patch, which gives low speed directional stability, should also give rise to a sinuous steered path in other speed ranges. The application of special interest to the authors is the problem of motorcycle instability.

A motorcycle can be considered as two castors coupled at the steering head (fig.1). The short trail, front castor gives rise to steering wobble (sometimes called 'flutter') of 6 - 8 Hz at 50 - 80 km/h, and the long trail, rear castor can initiate weave of the whole machine at 2 - 3 Hz over 130 km/h. This latter statement is a simplification in that it ignores coupling between the castors, but it is nevertheless an important notion in understanding the overall oscillatory behaviour of the vehicle. Both of these castor instabilities, wobble and weave, can be dangerous, even fatal, and have been the concern of manufacturers for many years.

The present discussion will concentrate on an isolated fixed-axis castoring wheel, and the motorcycle front wheel, with its subsequent wobble, will be used for later illustration. Changes in wobble characteristics have been observed with variation of wheel layout geometry, inertia distribution, wheel loading, road surface condition, and most important of all with lateral stiffness of the wheel mounting (1)*.

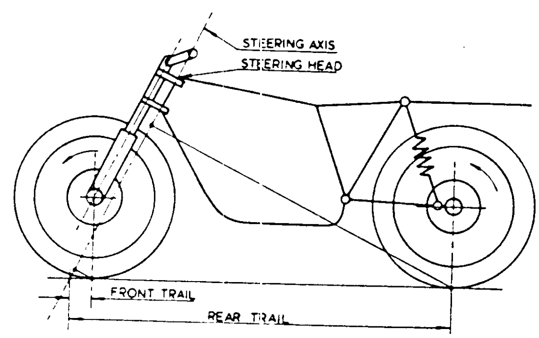

Fig. 1 - Motorcycle shown as two coupled castors

Most early studies of the problem predicted instability via tyre wall flexure, especially with aircraft landing gear (2) and motorcar front wheels (3). Roe (4) showed this to be

*Numbers in parentheses designate references at the end of the paper.

ABSTRACT

Castor oscillations are of prime importance in many situations, from the simple tea-trolley to towed vehicles, the landing wheels of aircraft, and the motorcycle instability problem of 'speed wobbles'. This paper sets out a mechanism of castor instability based on the lateral flexibility in the wheel support. In the case of a motorcycle this is the flexibility in the front fork/wheel system.

For small amplitude oscillations the equations of motion are shown to be coupled ordinary differential equations which contain terms representing a relay switching function. These equations are solved numerically for many parameter variations. Close agreement is obtained with observed amplitudes and frequencies, and with the oscillation characteristics. For certain sets of parameters the numerical solutions are also found to agree well with the predicted solutions obtained using an analytic technique.

From the results it is very clear that the most important parameter affecting stability is lateral stiffness, and a new motorcycle front fork of high lateral stiffness is described. This fork has already achieved success on the road, test track and race track.

SAE/SP-78/428/$02.50

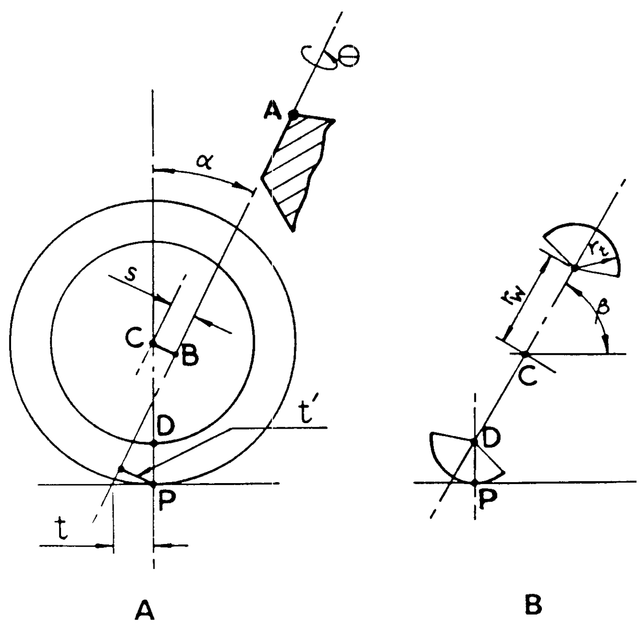

Fig. 2 - Basic geometry; A) wheel in vertical plane, θ=0, B) view along wheel plane showing inclined wheel at non-zero θ

only a special case of a more general instability mechanism due to lateral flexibility, and Roe & Thorpe (5) carried out model tests to verify these ideas, using wheels without a tyre. Sharp (6) has now included lateral frame flexibility in his computer analysis of motorcycle control(7).

The analysis described here will assume a rigid tyre and perfect 'hard' contact with the ground (friction force proportional to normal load), to demonstrate that tyre performance is not the only factor which can cause the instability mechanism to arise. Indeed with the tea-trolley wobble there is no pneumatic tyre to cause such oscillation anyway, and this hard contact model is directly applicable. In the case of road vehicles, the tyre does have one important effect - it provides hysteresis damping. In following the idealised model below, one can therefore reasonably assume that small amplitude oscillation would be damped out in the real situation. Lateral flexibility of wheel support (i.e. wheel rim support) will be provided by allowing a rigid wheel to slide laterally on its axle a displacement δ against springs of stiffness k . In the real situation this stiffness would arise from suspension components and the wheel structure itself. For the motorcycle, lateral flexibility at the front wheel arises principally via differential action in the 'telescopic' front fork legs.

2. BASIC CASTOR GEOMETRY.

The overall 'handling' of the vehicle is set by choosing empirically rake angle α (fig.2) and offset s to give trail t. The effective moment arm for lateral forces at the contact patch P is the perpendicular trail t'. Rotation about the steering axis is θ, assumed small. A wobble of $\pm 5^{\circ}$ is very severe, even catastrophic.

When the wheel is turned through θ about an inclined axis, at α , its plane moves out of the vertical. Its angle to the horizontal is β , where

$$\cos\beta = \sin\alpha \sin\theta \qquad (1)$$

Since castor instabilities are essentially lateral, the vehicle itself is not permitted to camber out of the vertical in this analysis. The height of the steering head above the ground is

$$H = AB\cos\alpha - s\sin\alpha\cos\theta + r_t + r_w\sin\beta \qquad (2)$$

where r_w is the wheel radius, and r_t is the radius of curvature of the tyre profile.

As the wheel is turned out of the straight-ahead position ($\theta = 0$) the steering head thus <u>falls</u> by an amount

$$\begin{aligned}\Delta H &= r_w(1 - \sin\beta) - s\sin\alpha(1 - \cos\theta)\\ &= \tfrac{1}{2}\theta^2\sin\alpha\,(r_w\sin\alpha - s) \qquad (3)\end{aligned}$$

for small θ. Now trail is conventionally defined in the $\theta = 0$ view, viz

$$t_o = (r_w\sin\alpha - s)/\cos\alpha + r_t\tan\alpha \qquad (4)$$

So if $r_w\sin\alpha > s$, i.e. $t_o > r_t\tan\alpha$ and the steering axis intersects the 'rolling radius' CP above the centre of curvature D, the steering head will <u>fall</u> on turning the steering from the straight-ahead position. There has been some dispute over this conclusion, and it is important, for since the centre of gravity of the whole vehicle will take up the position of lowest potential energy, the weight of the vehicle will cause the front wheel to turn away from the θ=0 position, for the above condition is usually satisfied in motorcycle practice. This therefore provides a 'decentralising' couple, and not the centralising couple often claimed to give 'weight assisted stability'. This decentralising couple does not in fact make a major contribution to castor stability, as will be seen later, but it is important to the 'handling' of the machine when the trail is large and/or the front wheel loading is high.

As the wheel is turned from θ = 0, the effective trail changes. Fig.3 shows the view at right angles to the wheel in this case. The effective rake angle is now γ , the projection of α about the steering axis through θ, viz

$$\tan\gamma = \tan\alpha\cos\theta \qquad (5)$$

In the θ = 0 position, the perpendicular trail is, from (4)

$$t_o' = (r_w + r_t)\sin\alpha - s \qquad (6)$$

In the turned position, the perpendicular trail becomes compounded from

$$t' = \begin{cases} (r_w + r_t\sin\beta)\sin\gamma - s & \text{in wheel plane} \\ r_t\cos\beta & \text{at right angles to wheel plane} \end{cases} \qquad (7)$$

The wheel plane component can be written as

$(r_w + r_t \sin\beta)\sin\alpha(1 + \cos^2\alpha\tan^2\theta)^{-\frac{1}{2}} - s$, and this passes through zero at a steering angle $\theta < 90^\circ$. Cornering, under a lateral force at the contact patch, becomes 'statically' unstable when this component of t' becomes negative, for the cornering force turns the wheel further into the curve. Fortunately, for conventional geometry this does not happen within the available range of θ.

3. MOTION OF THE CONTACT PATCH, WITH VERTICAL STEERING AXIS.

The simplest possible model of friction will be used, with the slip frictional force proportional to the normal load reaction R. The constant of proportionality is the dynamic coefficient of friction μ. In direction the frictional force opposes the velocity of slip. Fig.4 shows the resulting frictional forces at the contact patch in the plane of the road, with (a) wheel locked and (b) wheel free to rotate. v is the forward velocity of the vehicle. In (a) the resultant slip velocity is $V = [v^2 + (t\dot\theta)^2 + 2vt\dot\theta\sin\theta]^{\frac{1}{2}}$, and in (b) the resultant is $V' = [(2v\sin\frac{\theta}{2})^2 + (t\dot\theta)^2 + 4vt\dot\theta\sin\frac{\theta}{2}\cos\frac{\theta}{2}]^{\frac{1}{2}}$.

The resulting equation of motion for the wheel locked case is obtained by taking moments about the steering axis, viz

$$I\ddot\theta = -\frac{t^2\dot\theta\mu R}{V} - \frac{vt\sin\theta\mu R}{V} \qquad (8)$$

where I is the moment of inertia of wheel + supporting fork about the steering axis. For small θ,

$$I\ddot\theta + \frac{\mu R t^2\dot\theta}{[v^2 + (t\dot\theta)^2]^{\frac{1}{2}}} + \frac{\mu R v t\theta}{[v^2 + (t\dot\theta)^2]^{\frac{1}{2}}} = 0 \qquad (9)$$

To interpret this, take the usual case of $v^2 \gg (t\dot\theta)^2$, for then

$$\underline{I\ddot\theta + (\frac{\mu R t^2}{v})\dot\theta + (\mu R t)\theta = 0} \qquad (10)$$

This, surprisingly, is the standard form for viscous damped single degree of freedom vibration. Typical magnitudes show damping to be well below critical, so any small oscillation of steering angle θ is inherently stable under the assumptions noted.

Permitting the wheel to rotate gives the equation of motion

$$I\ddot\theta = -\frac{t^2\dot\theta\mu R}{V'} - \frac{2vt\sin\frac{\theta}{2}\cos\frac{\theta}{2}\mu R}{V'}. \qquad (11)$$

For small θ, $V' = [v^2\theta^2 + (t\dot\theta)^2 + 2vt\dot\theta\theta]^{\frac{1}{2}} = |v\theta + t\dot\theta|$. So

$$I\ddot\theta + \frac{(t\dot\theta)\mu Rt}{|v\theta + t\dot\theta|} + \frac{(v\theta)\mu Rt}{|v\theta + t\dot\theta|} = 0$$

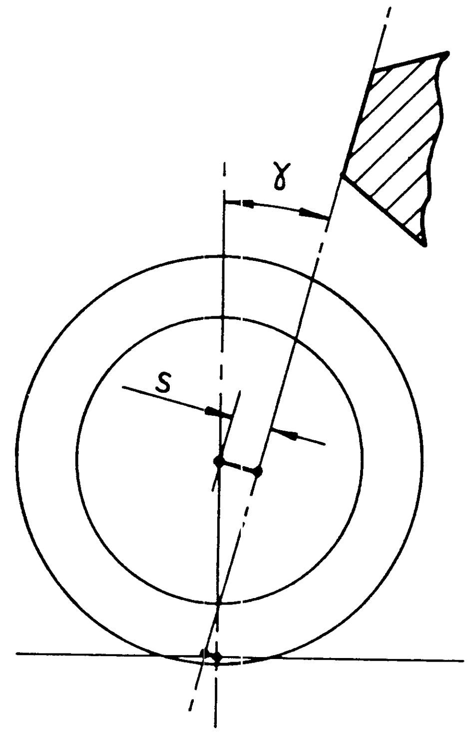

Fig. 3 - View at right-angles to wheel with steering in turned position ($\theta \neq 0$)

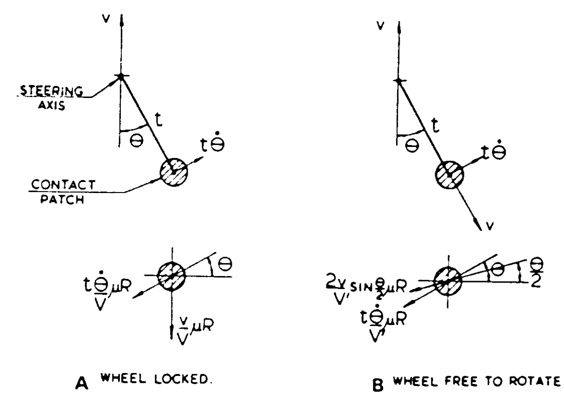

Fig. 4 - Motion of contact patch, and components of contact patch force; A) wheel locked, B) wheel free to rotate

i.e.

$$\underline{I\ddot\theta + \mu Rt\epsilon = 0} \qquad (12)$$

where $\epsilon = \dfrac{\theta + \frac{t}{v}\dot\theta}{\left|\theta + \frac{t}{v}\dot\theta\right|}$, a unit quantity with the sign of $\theta + \frac{t}{v}\dot\theta$. (13)

The contact patch frictional force thus acts approximately at right angles to the wheel plane, giving a couple μRt with sign changes controlled by ϵ.

Equation (12) has been solved by both analogue and digital methods, and found to give damped oscillation after any initial perturbation. ϵ has the effect of giving hysteresis damping. The system is therefore again inherently stable.

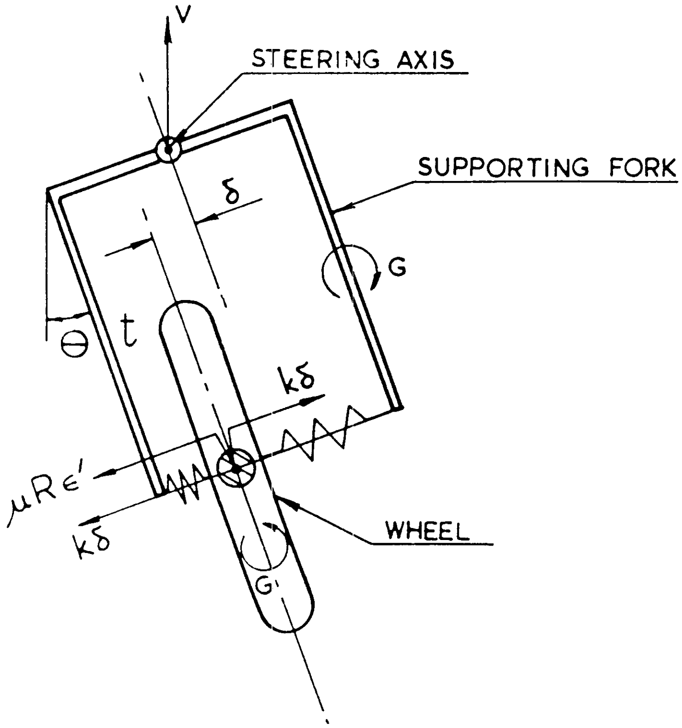

Fig. 5 - Flexible castor, vertical steering axis

In fig.5, G is the reaction couple of the wheel on its axle. The wheel has mass M_w and moment of inertia I_{wo} about an axis through its centre parallel to the steering axis. The supporting fork has a moment of inertia I_s about the steering axis.

The equations of motion are

$$M_w(t\ddot{\theta} - \ddot{\delta}) = k\delta - \mu R\epsilon'$$

$$I_{wo}\ddot{\theta} = G$$

$$I_s\ddot{\theta} = -G - tk\delta$$

which may be written as

$$(I_s + I_{wo})\ddot{\theta} = -tk\delta$$

$$M_w t^2\ddot{\theta} - M_w t\ddot{\delta} = tk\delta - \mu Rt\epsilon' \qquad (16)$$

These equations do indeed allow unstable oscillation in θ, i.e. castor oscillation, and the solution will be described later as the special case of zero rake angle α. An energy argument showing how such a flexible castor might be unstable has been presented by Roe (4).

4. STEERING OSCILLATIONS WHEN THE WHEEL IS PERMITTED TO MOVE LATERALLY IN ITS SUPPORTING FORK, WITH VERTICAL STEERING AXIS.

Observations from high speed film of castor oscillation showed the wheel to make a cyclic movement along its axle in the 'free play' available. Moreover, reduction in this sideplay produced a more stable castor. The above theoretical model was therefore modified to incorporate this sideplay δ (fig.5). The model used by [illegible] ([illegible]) includes a parameter called 'wheel bearing play', but this does not permit any relative movement of wheel and supporting fork. Unrestricted lateral movement of the wheel within the fork was not analysed here because of complications at the impact of wheel and fork at the ends of the free play twice per cycle, rather the wheel was restrained by axle springs of stiffness k. The latter case is also more appropriate to the vehicle case, where it is flexibility in the wheel support which creates the greatest stability problem, although some unrestricted play may also exist due, for example, to loose or worn wheel bearings, or sliding clearance in the case of a telescopic motorcycle fork.

The analysis is similar to that above, but one must now distinguish between the steering angle θ, and the angular position of the contact patch,

$$\theta_c = \theta - \frac{\delta}{t} \qquad (14)$$

Also, ε becomes

$$\epsilon' = \frac{\theta + \frac{t}{V}\dot{\theta}_c}{\left|\theta + \frac{t}{V}\dot{\theta}_c\right|} = \frac{\theta + \frac{t}{V}\dot{\theta} - \frac{\dot{\delta}}{V}}{\left|\theta + \frac{t}{V}\dot{\theta} - \frac{\dot{\delta}}{V}\right|} \qquad (15)$$

5. THE CASE OF AN INCLINED STEERING AXIS - THE FINAL EQUATIONS.

With reference to fig.6, assume $\theta \ll 1$ and $\delta/t' \ll 1$, i.e. look for small amplitude oscillations as before. The contact patch force at right angles to the wheel plane (wheel now cambered as well as steered) is

$$\mu\epsilon' R\sin\beta - R\cos\beta = R(\mu\epsilon' - \theta\sin\alpha) \qquad (17)$$

to first order in θ

The contact patch force in the plane of the wheel gives a restoring couple

$$(\mu\epsilon' R\cos\beta + R\sin\beta)\sin\gamma.\delta = R\sin\alpha.\delta \qquad (18)$$

to first order in δ & θ.

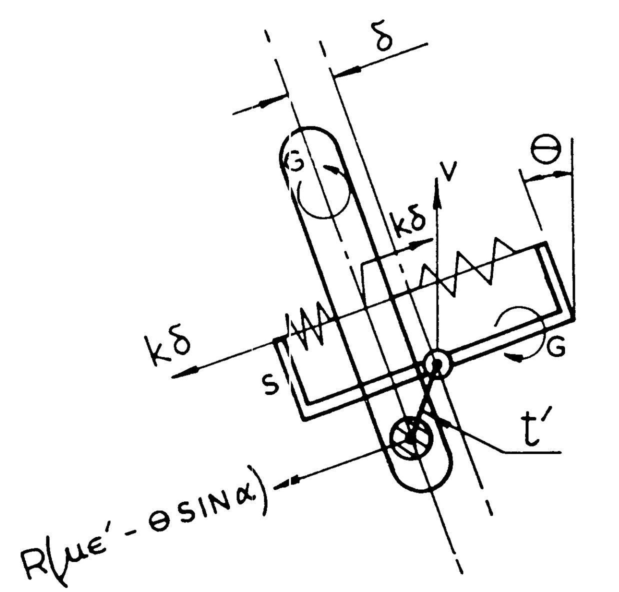

Fig. 6 - Flexible castor; view down steering axis of inclined axis case

Changes in t' are of second order in θ and will be neglected. In ϵ', t is replaced by t'. The new equations of motion are therefore

$$M_w(s\ddot{\theta} + \ddot{\delta}) = -k\delta + R(\mu\epsilon' - \theta\sin\alpha) + M_w g\theta\sin$$

$$I_{wo}\ddot{\theta} = G - R(\mu\epsilon' - \theta\sin\alpha)(t' + s)$$

$$I_s\ddot{\theta} = -G + sk\delta + M_s gh\theta\sin\alpha - R\sin\alpha.\delta \qquad (19)$$

which may be written as

$$(I_s + I_{wo})\ddot{\theta} = sk\delta - R(\mu\epsilon' - \theta\sin\alpha)(t' + s) + M_s gh\theta\sin\alpha - R\sin\alpha.\delta$$

$$M_w s^2\ddot{\theta} + M_w s\ddot{\delta} = -sk\delta + sR(\mu\epsilon' - \theta\sin\alpha) + M_w gs\theta\sin\alpha \qquad (20)$$

Putting $\alpha = 0$ and t' = t = -s in (20) recovers the vertical axis equations as in (16).

Equations (20) are the basic equations to be solved, over a range of parameters.

6. THE RANGE OF PARAMETERS USED.

The details are given in fig.7, but some comment on reasons for the given choice is worthwhile. The basic values in fig.7 correspond to typical motorcycle practice, for the front wheel.

Rake α is varied, at constant trail, for this is often changed by manufacturers seeking better stability. The usual value is $\alpha \doteq 25^\circ$, but current trend is towards 30°. In this analysis α is taken from 0° (vertical steering axis) to 25°.

Case.	I_s kg m^2	I_{wo} kg m^2	M_s kg	M_w kg	k N/m	deg	s m	v m/s		R N	g m/s^2	h m
1.	0.125	0.540	10	10	10^5	0	-0.07678	20	1	1250	9.8	0
2.	0.125	0.540	10	10	10^5	10	-0.02468	20	1	1250	9.8	0
3.	0.125	0.540	10	10	10^5	14.83	0	20	1	1250	9.8	0
4.	0.125	0.540	10	10	10^5	20	0.02583	20	1	1250	9.8	0
5.	0.125	0.540	10	10	10^5	25	0.05000	20	1	1250	9.8	0
6.	0.125	0.540	10	10	10^5	25	0.05000	20	1	1250	9.8	0.05000
7.	0.125	0.540	10	10	10^5	25	0.05000	20	1	1250	0	0
8.	0.125	0.540	10	10	10^5	25	0.05000	20	0.5	1250	9.8	0
9.	0.125	0.540	10	10	10^5	25	0.05000	20	1	2500	9.8	0
10.	0.125	0.540	10	10	10^5	25	0.05000	20	1	625	9.8	0
11.	0.125	0.540	10	10	10^5	25	0.05000	10	1	1250	9.8	0
12.	0.125	0.540	10	10	10^5	25	0.05000	30	1	1250	9.8	0
13.	0.125	0.540	10	10	10^5	25	0.05000	40	1	1250	9.8	0
14.	0.125	0.540	10	10	10^5	0	-0.15000	20	1	1250	9.8	0
15.	0.125	0.540	10	10	10^5	25	-0.07678	20	1	1250	9.8	0
16.	0.125	0.540	10	10	10^4	0	-0.07678	20	1	1250	9.8	0
17.	0.125	0.540	10	10	10^6	0	-0.07678	20	1	1250	9.8	0
18.	0.125	0.540	10	10	10^4	25	0.05000	20	1	1250	9.8	0
19.	0.125	0.540	10	10	10^6	25	0.05000	20	1	1250	9.8	0
20.	0.125	1.080	10	20	10^5	25	0.05000	20	1	1250	9.8	0
21.	0.250	0.540	20	10	10^5	25	0.05000	20	1	1250	9.8	0
22.	as 11, but with small initial displacement.											
23.	as 5 , " " " " "											
24.	as 12, " " " " "											
25.	as 13, " " " " "											

Fig. 7 - Table of parameters used for solution

There is some current discussion about the effect of mass distribution in the front fork, and here h is changed to move the fork centre of gravity. The inclusion or omission of the gravitational acceleration g allows study of the 'pendulum effect' of the front wheel + fork, about the steering axis (in fact an inverted pendulum giving a decentralising couple). This is not to be confused with the decentralising couple from 'rise and fall' of the steering head (section 2) which enters the equations via R and non-zero α.

The coefficient of friction is for slip, and two values are used 1 and 0.5, for dry and wet surfaces respectively. The normal wheel load reaction R is varied to simulate the effect of weight transfer under acceleration and braking, low R and high R respectively.

Several values of forward velocity v are studied, as experimentally observed wheel wobble occurs in a fairly well defined speed range of 50 - 80 km/h (30 - 50 mph).

Another design parameter often changed by manufacturers is trail, with longer trails generally giving higher stability, if also more difficult steering (section 2).

The most important variable is k, the lateral stiffness of wheel support, here simulated by axle springs. Current front forks are not particularly stiff laterally, typically $k \doteq 10^{[illegible]}$ N/m as used here. More recent experimental forks by Roe & Thorpe, described later, have increased this by a factor of 4 - 5, with substantial improvement in stability.

The remaining variations are concerned with mass and inertia of wheel and fork. Model tests ([illegible]) showed an increase in fork inertia about the steering axis to decrease stability.

All these calculation cases, with the exception of 22-25, have the same starting conditions of $\theta = 0.2$ rad, $\dot{\theta} = 0$, $\delta = 0.01$ m, $\dot{\delta} = 0$, i.e. steering angle and sideplay are given finite perturbation, and then the system is released from rest. Cases 22-25 repeat the velocity scan runs 11,5,12 & 13, but with an infinitesimal starting condition of $\theta = 10^{-5}$ rad, $\dot{\theta} = 0$, $\delta = 10^{[illegible]}$ m, $\dot{\delta} = 0$, in an attempt to simulate the steady build up of wobble observed when a rider simply releases control from the steering on an almost smooth road surface.

On reading fig.7, and the resulting oscillations, it should be noted that case 5 (and 25 for small perturbations) corresponds most closely with existing motorcycle production practice.

7. ANALYSIS OF THE EQUATIONS.

By eliminating $\ddot{\theta}$ from the second of (20) one obtains

$$\ddot{\theta} = a\delta + b\theta + c\epsilon' \tag{21}$$

and

$$\ddot{\delta} = l\delta + m\theta + n\epsilon' \tag{22}$$

where

$$a = (sk - R\sin\alpha)/(I_s + I_{wo}),$$
$$b = [(t' + s)R + M_s gh]\sin\alpha/(I_s + I_{wo}),$$
$$c = -(t' + s)\mu R/(I_s + I_{wo}),$$
$$l = -sa - k/M_w \tag{23}$$
$$m = (g - R/M_w)\sin\alpha - sb,$$

and $n = \mu R/M_w - sc$.

From (14) & (15) it follows that

$$\epsilon' = \mathrm{sgn}(\theta + d\dot{\theta} - e\dot{\delta}) , \tag{24}$$

where $d = t'/v$, $e = 1/v$ (25)

Any solution of (21) and (22) must take proper account of the presence of the relay switching function, that is the terms involving ϵ'. In particular, as discussed by Flügge-Lotz (8), André and Seibert (9) and Anderson & Moore (10) it is insufficient with relay systems to define sgn(0) as zero, and the situation

$$\theta + d\dot{\theta} - e\dot{\delta} = 0 \tag{26}$$

requires special interpretation. In order to analyse this further it is convenient to use matrix notation with the following definitions :

$$\underset{\sim}{x} = (\theta,\dot{\theta},\delta,\dot{\delta})^T , \tag{27}$$
$$\underset{\sim}{q} = (1,d,0,-e)^T , \tag{28}$$
$$\underset{\sim}{u} = -(0,c,0,n)^T , \tag{29}$$

where $(\ )^T$ denotes transpose, and

$$A = \begin{pmatrix} 0 & 1 & 0 & 0 \\ b & c & a & 0 \\ 0 & 0 & 0 & 1 \\ m & 0 & l & 0 \end{pmatrix} \tag{30}$$

so that (21) and (22) may be written as

$$\dot{\underset{\sim}{x}} = A\underset{\sim}{x} - \underset{\sim}{u}\,\mathrm{sgn}(\underset{\sim}{q}^T\underset{\sim}{x}) . \tag{31}$$

The state space of the variables θ, $\dot{\theta}$, δ and $\dot{\delta}$ is divided into two regions by the switching surface or hyperplane $\underset{\sim}{q}^T\underset{\sim}{x} = 0$ (equation (26)). In one region $\mathrm{sgn}(\underset{\sim}{q}^T\underset{\sim}{x}) = 1$, in the other $\mathrm{sgn}(\underset{\sim}{q}^T\underset{\sim}{x}) = -1$ and in both these regions the states move according to (31). This type of motion is usually called the 'bang-bang' mode. However, as described in detail in ref (10), motion along the switching surface ('sliding' motion) is also possible if the condition

$$\left|\underset{\sim}{q}^T A\underset{\sim}{x}\right| < \underset{\sim}{q}^T\underset{\sim}{u} \tag{32}$$

is satisfied (together with $\underset{\sim}{q}^T\underset{\sim}{x} = 0$) and the states then move according to

$$\dot{\underset{\sim}{x}} = \underset{\sim}{f}^+ - (\underset{\sim}{f}^- - \underset{\sim}{f}^+)\underset{\sim}{q}^T\underset{\sim}{f}^+ / \underset{\sim}{q}^T(\underset{\sim}{f}^- - \underset{\sim}{f}^+) , \tag{33}$$

where $\underset{\sim}{f}^+ = A\underset{\sim}{x} - \underset{\sim}{u}$
and $\underset{\sim}{f}^- = A\underset{\sim}{x} + \underset{\sim}{u}$ (34)

For the system (31)

$$\underset{\sim}{q}^T\underset{\sim}{u} = \frac{\mu R}{v}\left[\frac{1}{M_w} + \frac{(t' + s)^2}{I_s + I_{wo}}\right] , \tag{35}$$

which clearly indicates that sliding motion can occur, and the system of linear ordinary differential equations describing this motion may easily be obtained from (33). Thus the complete solution of the problem consists of sliding and bang-bang motion, transfers from one type of motion to the other being determined by (32) and the value of $q^T x$ at any instant of time.

Analysis of the simple rigid model described by equation (12) shows that after an initial period of bang-bang motion sliding occurs in which θ and $\dot{\theta}$ decay exponentially to zero and no return to the bang-bang mode is possible. This is clearly in accord with the general physical arguments described in section 3.

8. NUMERICAL SOLUTION OF THE EQUATIONS.

Given θ, $\dot{\theta}$, δ, $\dot{\delta}$ at time T = 0 a numerical solution of the first order system (31) was obtained using an Adams-Bashforth predictor-corrector type method. The integration interval was automatically varied in order to ensure that the magnitude of the step-wise truncation error associated with each calculated state variable was less than some prescribed tolerance. The same method was used to solve the sliding equations derived from (33).

In order that transfers from the bang-bang mode to the sliding mode could be accurately accomplished, the equation

$$\dot{y}_1 = j\ \mathrm{sgn}(q^T x) \tag{36}$$

was solved during the bang-bang motion in addition to (31), assuming $y_1 = 0$ at T = 0 and j = 1. When the switching surface was crossed, say $\mathrm{sgn}(q^T x)$ changed from +1 to -1, the integration of (31) and (36) was stopped and restarted from the previously calculated point in state space for which $\mathrm{sgn}(q^T x) = 1$ but now with j = 10. This has the effect of increasing the calculated value of the differences of y_1 as the switching surface is crossed (compared with the case j = 1). Since, for the method used, the estimate of the step-wise truncation error associated with (36) is based on difference formulae, for j = 10 the integration interval in T was automatically reduced in order to reduce the magnitude of this truncation error to within the prescribed tolerance. This procedure was repeated with a sequence of increasing values of j in order to approach the switching surface $q^T x = 0$ as closely as desired. Once this was achieved (32) was examined to determine whether the subsequent behaviour was governed by the sliding or bang-bang mode. If sliding were indicated, the latest calculated values of the state variables served as initial conditions to begin the integration of (33), otherwise the integration of (31) and (36) was continued.

A similar technique was used to ensure accurate transfer from sliding to bang-bang mode, the extra equation in this case being chosen as

$$\dot{y}_1 = j\ \mathrm{sgn}(q^T u - |q^T A x|)\ . \tag{37}$$

In all these calculations the upper limit on the magnitude of the truncation error was chosen to be 1 unit in the fifth decimal place with $|q^T x| < 10^{-5}$ regarded as the switching surface.

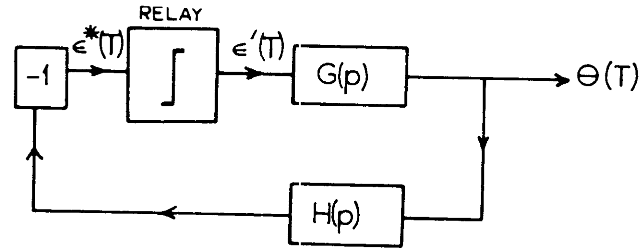

Fig. 8 - Block diagram of system

9. THEORETICAL ANALYSIS OF LIMIT-CYCLE OSCILLATIONS.

The characteristics of steady-state limit-cycle oscillations as a function of system parameters can be predicted using frequency response techniques (11). The system model equations (21) - (25) are transformed into the Laplace complex frequency plane and the system can then be represented as shown in the block diagram fig.8 with a relay non-linearity (12). G(p) and H(p) are rational transfer functions such that

$$G(p) = \frac{\beta_1 + \beta_2 p^2}{\alpha_1 + \alpha_2 p^2 + \alpha_3 p^4} \tag{38}$$

$$\text{and}\quad G(p)H(p) = \frac{\beta_1 + \beta_3 p + \beta_2 p^2 + \beta_4 p^3}{\alpha_1 + \alpha_2 p^2 + \alpha_3 p^4} \tag{39}$$

where the constants α_i and β_i can be expressed in terms of the system parameters (23) and (25).

The sinusoidal describing function method (13), which is often used to predict limit-cycles, assumes that the oscillation can be approximated by a sine wave with the non-linearity replaced by an equivalent linear gain factor. In our case, however, higher harmonics cannot be neglected since the system does not attenuate the higher frequency signals sufficiently.

An 'exact' method (14) will be used to investigate the presence of symmetric 'simple' limit-cycles. The relay is assumed to change sign once every half cycle during the oscillation period. Then the non-linearity output is a square wave

$$\epsilon'(T) = U(T) - 2U(T - \tfrac{1}{2}T_o) + 2U(T - T_o) - 2U(T - \tfrac{3}{2}T_o) + \ldots \tag{40}$$

where $U(T - \tau)$ is the displaced unit step function having value 1 for $T > \tau$ and 0 for $T < \tau$. T_o is the period of the oscillation. For $T \geq 0$, the Fourier series of (40) is

$$\epsilon'(T) = \frac{4}{\pi}\sum_{k\ \mathrm{odd}}^{\infty} \frac{\sin(k\omega_o T)}{k} = \frac{4}{\pi}\sum_{k\ \mathrm{odd}}^{\infty} \frac{1}{k}\,\mathcal{Im}\, e^{ik\omega_o T}$$

with $\omega_o = 2\pi/T_o$. (41)

The waveform $\epsilon'(T)$ produces the input to the relay non-linearity

$$\epsilon^*(T) = -\frac{4}{\pi}\sum_{k\ \mathrm{odd}}^{\infty} \frac{1}{k}\,\mathcal{Im}\left[G(ik\omega_o)\, H(ik\omega_o)\, e^{ik\omega_o T}\right], \tag{42}$$

using the properties of system frequency transfer functions (12).

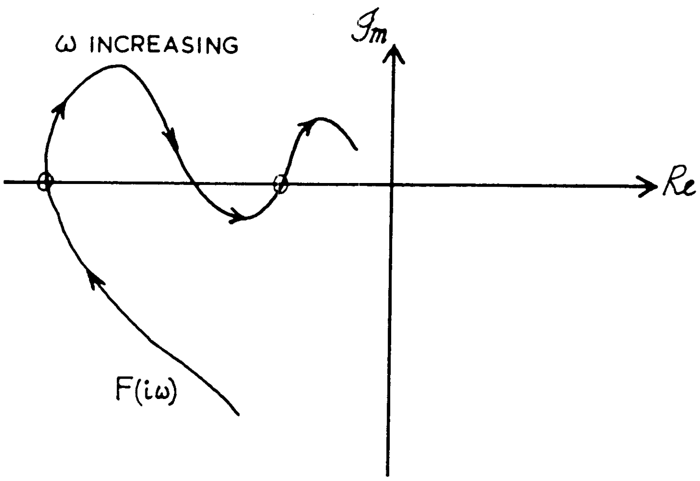

Fig. 9 - Tsypkin locus; 0 indicates stable limit-cycle point

It is required at time $T_1 = \lim_{\delta \to 0}(T_o/2 - \delta)$ that $\epsilon^*(T_1) = 0$ and $\frac{d\epsilon^*}{dT}(T_1) < 0$ (43)
for the oscillation to exist. These conditions require that the value of $\epsilon^*(T)$ at the half period is equal to the value of $\epsilon^*(T)$ at the period outset, and that the slopes are reversed at these times.

The Tsypkin locus (14) is defined to be the plot of the complex function

$$F(i\omega) = \sum_{k\ odd}^{\infty} \mathcal{R}e[G(ik\omega)\ H(ik\omega)] + i \sum_{k\ odd}^{\infty} \frac{1}{k} \mathcal{I}m[G(ik\omega)\ H(ik\omega)] \qquad (44)$$

as ω is varied from zero to infinity. From (42), (43) and (44) the necessary conditions for a symmetric oscillation to exist at the frequency $f_o = 2\pi\omega_o$ Hz can be shown to be (11)

$$\mathcal{I}m[F(i\omega_o)] = 0$$
$$\mathcal{R}e[F(i\omega_o)] < \lambda \qquad (45)$$

where, for the system under consideration,

$$\lambda = \frac{\pi}{4\omega_o} \lim_{p\to 0}[pG(p)\ H(p)] = 0 \qquad (46)$$

The Tsypkin locus can be plotted on the complex plane. The expressions (45) indicate that limit-cycles exist for values of ω_o giving points on the Tsypkin locus on the negative real axis. Furthermore, for the oscillation to be stable it is necessary that (15)

$$\frac{d}{d\omega}[\mathcal{I}m\ F(i\omega)]\Big|_{\omega=\omega_o} > 0 \qquad (47)$$

The existence of stable limit-cycles can be predicted as shown in fig.9 . The particular limit-cycle which is generated in the steady state is determined by the initial values of the system variables at T = 0.

The waveforms of all the system variables can be determined for an oscillation of given frequency from equations similar to (42). Using equation (32) one must investigate whether sliding motion occurs at the time when the non-linearity input $\epsilon^*(T)$ changes sign. If the

Case	Amplitude (degrees) theory	Amplitude (degrees) simulation	Frequency (Hz) theory	Frequency (Hz) simulation	% sliding
1.	4.4	4.5	[illegible]	8.5	21
[illegible]	[illegible]	[illegible]	8.7	8.5	20
3.	5.6	[illegible]	[illegible]	8.1	22
5.	2.5	[illegible]	8.7	[illegible]	30
14.	[illegible]	[illegible]	[illegible]	9.3	5

Fig. 10 - Comparison of theoretical and simulated oscillation characteristics for infinitesimal initial conditions

sliding conditions are satisfied, sliding motion commences and our assumption of a 'simple' limit-cycle with a single sign change in $\epsilon'(T)$ once every half cycle is invalid. A short sliding time relative to the oscillation period indicates that the limit-cycle predicted by the Tsypkin locus technique is closely approximated by the actual system oscillation. The possibility of sliding motion has not been noted in the literature with regard to the prediction of limit-cycles using frequency response techniques.

The peak amplitude and frequencies of the limit-cycles determined by the above theoretical technique and the numerical simulations of section 8 are compared in fig.10 . When the sliding motion occupies a small fraction of the oscillation period, the predicted and the simulated limit-cycles are very close. For longer sliding times the results differ, but are still of the same order of magnitude.

10. DISCUSSION OF RESULTS.

The results of section 8 are presented graphically in fig.11, as oscillations of steering angle θ. A typical δ oscillation is also shown (case 6).

All cases show castor oscillation, in the frequency range 5 - 9 Hz depending on the choice of parameters. This corresponds very closely with the real case of 6 - 8 Hz. Also in the real case tyre hysteresis damping is present, so one can reasonably assume that a small amplitude oscillation from this analysis might well be damped out in the real situation. Only the simplest model of wheel/road friction was used, and deliberately so, to demonstrate that the properties of a pneumatic tyre are not essential to castor oscillation.

Motion started with a large perturbation is characterised by large unsteady transients, followed by smaller, constant amplitude steady state oscillation. Motion started with a small perturbation shows only the limit-cycle steady state shimmy. Although this is of apparently small amplitude, it must be remembered that a wobble of $\pm 5^\circ$ is highly dangerous. For stability in the real situation, one should look for a rapid decay of transients and a very small

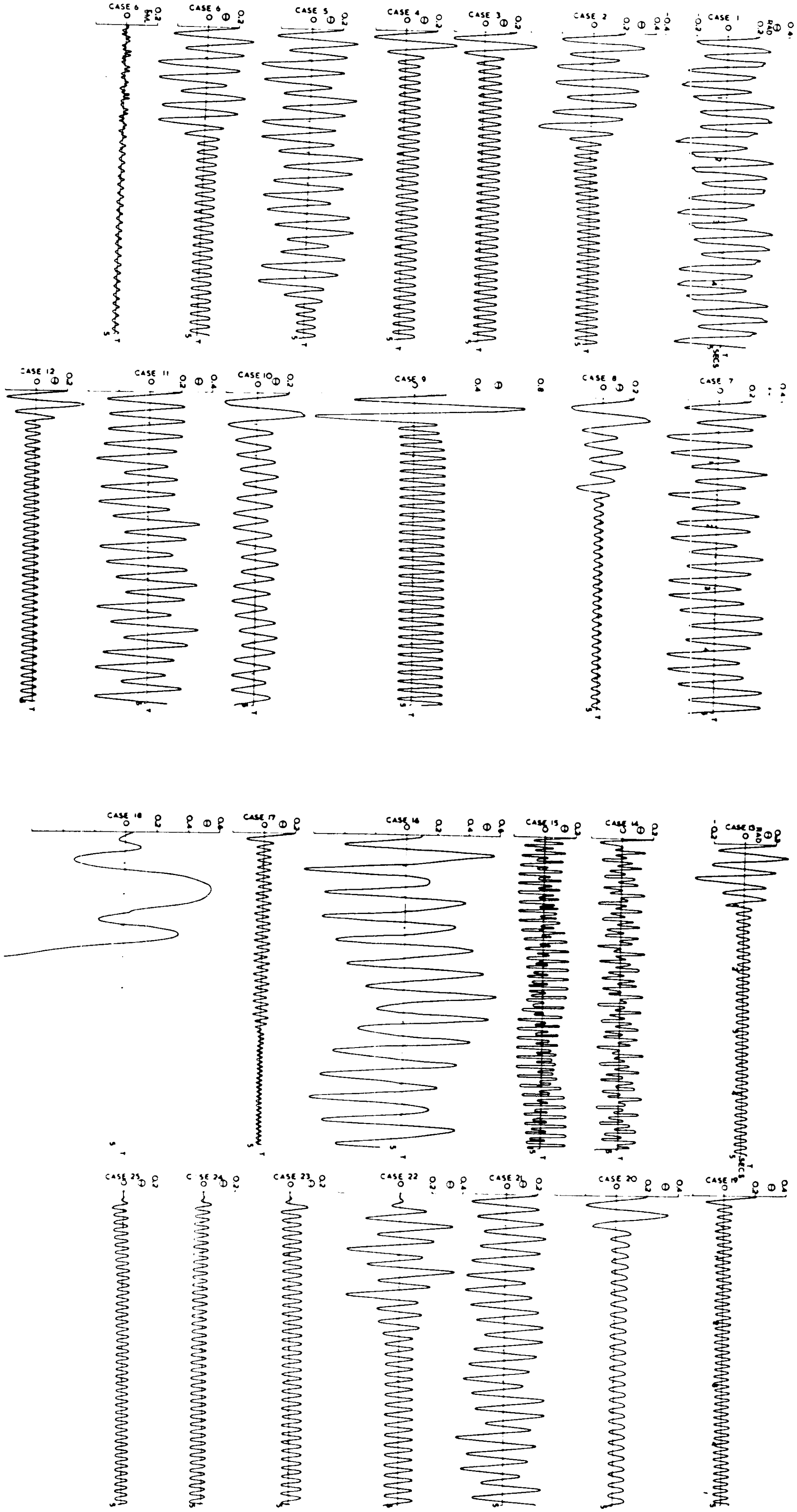

Fig. 11 - θ oscillations under parameter variation (case 6 shows δ oscillation also). See Fig. 7 for parameters used

steady state amplitude in these results.

Parameter variation gives the following conclusions.

(i) α, with t' constant [cases 1-5]. The quickest transient decay is for $\alpha = 15^\circ$ or 20°, but the lowest steady state amplitude ($\pm 3.6^\circ$) is at $\alpha = 25^\circ$.

(ii) h [case 6, with 5]. Increasing h (distance of fork centre of gravity ahead of steering axis) causes transients to decay more quickly.

(iii) g [case 7, with 5]. Removal of 'pendulum effect' (putting g=0) delays transient decay.

(iv) μ [case 8, with 5]. Reducing μ (slippery surface) reduces amplitudes via lower driving force, but in real system available damping is also much lower.

(v) R [cases 9,10 with 5]. Very large oscillation amplitude when wheel load R is increased, but steady state established more quickly. In practice the loading up of an unstable wheel, e.g. by weight transfer, can produce alarming amplitudes.

(vi) v [cases 11,5,12 & 13 for increasing v]. Progressive slight stabilisation with increasing road speed. Case examined ($\alpha = 25^\circ$) shows distinct drift to stability between v = 20 and v = 30 m/s (45 & 65 mph). On the road, with damping, there is a transition back to stability between 45 & 55 mph. It is interesting that some transition is predicted here even without gyroscopic coupling (steering axis rigidly constrained).

(vii) t' [cases 14 with 1, 15 with 5]. Increase of trail reduces amplitude of oscillation, for $\alpha =$ [illegible] or $\alpha = 25^\circ$.

(viii) k [cases 16,1 & 17, and 18,5 & 19]. Lateral stiffness has the most dramatic influence on stability. A high k is most important, for $\alpha =$ [illegible] or $\alpha = 25^\circ$.

(ix) M_w [case 20, with 5]. Increase of wheel mass improves the decay of transients.

(x) I_3 [case 21, with 5]. Increase of fork inertia delays the decay of transients, i.e. decreases stability.

(xi) Small amplitude perturbation [cases 22 - 25, with (vi) above]. Apart from the loss of transients, the same behaviour with forward velocity v as for large initial perturbation.

Agreement with the real system is remarkably close for all parameter variation. The only exceptions are :

(a) Decrease in μ gives here a rather inconclusive effect, but in the real situation stability is decreased slightly via easier initiation of oscillation, and less damping.

(b) Although the transition towards stability with increasing v is predicted, the transition from stability at v=0 to instability at small v, found experimentally, is not indicated.

Both of these discrepancies can be explained if the rolling wheel has an initial reluctance to break away and slide laterally, to change from rolling to slipping. This would be expected physically, with the static value of the coefficient of friction being higher than the dynamic (slipping) value. Decreasing μ encourages slip and hence the initiation of oscillation. Also the more rapidly the wheel rotates (high v), the more longitudinal slip takes place, again encouraging lateral slip. The model analysed here assumes free slip, with a dynamic coefficient of friction.

This idea is supported by the reluctance of a highly loaded wheel (high R) to commence shimmy oscillation, although once disturbed a high-R wheel has a more violent oscillation (correctly predicted). Also, once a wheel is wobbling, the forward speed can often be dropped to virtually zero before oscillation stops.

The original proposition of lateral flexibility as the basic cause of instability is fully supported by these results, and indeed letting $k \to \infty$ in the equations of motion recovers the stable case discussed in section 3. Important secondary influences on the oscillation are trail, rake angle, steering inertia and wheel load.

11. APPLICATION TO THE DEVELOPMENT OF NEW MOTORCYCLE FRONT FORKS.

With this very decisive theoretical support, together with the results of the model tests mentioned earlier, the building of experimental motorcycle forks with high lateral stiffness became a high priority.

It is very difficult to achieve high lateral stiffness with the 'telescopic' type of fork in current vogue, as the running clearances in the sliding legs allow differential action between the two legs, even when they are rigidly connected (e.g. by a large diameter wheel spindle). Several alternative front wheel suspension systems were evaluated, and the most promising was the 'leading link' fork (fig.12) in which a large diameter (tubular) wheel spindle pivots on short stiff links about preloaded bearings. These bearings also take the braking loads and prevent 'spragging' of the suspension. The fork illustrated has a wheel travel of 150 mm, uses standard motorcycle steering geometry, and has approximately the same mass and steering inertia as the telescopic fork it replaces. Its lateral stiffness is however five times higher ! It is the latest of a development series, and has been given extensive testing on the road, test-track and race track.

Machines tested with this fork have no steering wobble ('flutter'), even when the machine is heavily laden with touring luggage. Moreover, there is no high speed weave either. In addition to stability improvement, there have also been substantial gains in suspension comfort, basic steering quality, and in the acceptance of higher braking forces with full rider control. In racing, this has led to significant reduction in lap times, with the race machine often lapping quicker than other machines of much greater horsepower. There seems little doubt that forks of this type, with this order of lateral stiffness, will feature in future motorcycle designs, if only for the improvement in basic safety.

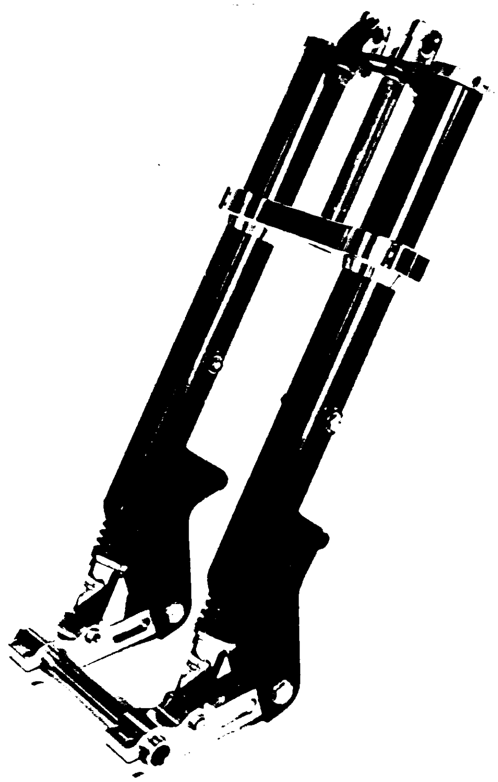

Fig. 12 - Motorcycle front fork with high lateral stiffness, and high stability

12. CONCLUSIONS.

A mechanism of castor oscillation is proposed based on lateral flexibility in the wheel support, without any dynamical contribution from a pneumatic tyre being necessary. Agreement with the real system of motorcycle front wheel wobble is extremely close, in amplitude, frequency and character of oscillation.

The model is analysed over a wide range of parameter variation, using (i) an entirely numerical approach allowing for both the sliding and bang-bang modes associated with relay systems, and (ii) the Tsypkin locus analytic technique ignoring sliding.

With the theoretical demonstration that high lateral stiffness of wheel support is needed for stability, a new stiff motorcycle fork has been developed giving total stability and improved handling. It has been extensively tested for both road and racing use.

NOTATION.

- g Gravitational acceleration.
- h Distance of fork centre of gravity ahead of steering axis.
- H Height of steering head.
- I_s Moment of inertia of supporting fork about steering axis.
- I_{wo} Moment of inertia of wheel about a diameter.
- k Stiffness of lateral wheel support in fork.
- M_s Mass of supporting fork.
- M_w Mass of wheel.
- r_t Radius of curvature of tyre profile.
- r_w Wheel radius, to centre of curvature of tyre profile.
- R Normal load reaction at wheel contact patch.
- s Wheel offset, forward of steering axis.
- t Trail
- t_o Trail in $\theta=0$ view.
- t_p Perpendicular trail.
- T Time
- v Forward velocity of vehicle.
- α Rake angle, to vertical.
- β Wheel camber angle, to horizontal.
- δ Lateral wheel deflection.
- ϵ, ϵ' Unit function determining sign-change point of contact patch frictional force.
- θ Steering angle, away from straight-ahead position.
- μ Coefficient of friction.
- γ Projection of α through θ.

REFERENCES.

1. G.E. Roe & T.E. Thorpe, "A solution of the low-speed wheel flutter instability in motorcycles". J.Mech.Eng.Sci. 18 No.2, p.57, 1976.
2. A. Kantrowitz, "Stability of castoring wheels for aircraft landing gears". Tech.Notes Nat.Advis.Comm.Aeronaut.Wash. 686, 1940.
3. H.B. Pacejka, "Analysis of shimmy phenomenon". Proc.I.Mech.E. 180(2A) p.251, 1966.
4. G.E. Roe, "Theory of castor oscillations". J.Mech.Eng.Sci. 15 No.5, p.379, 1973. Also Communication 17 No.1, p.42, 1975.
5. G.E. Roe & T.E. Thorpe, "Experimental investigation of the parameters affecting the castor stability of road wheels". J.Mech.Eng.Sci. 15 No.5, p.365, 1973.
6. R.S. Sharp, "The stability and control of motorcyles". J.Mech.Eng.Sci. 13 No.5, p.316, 1971.
7. R.S. Sharp, "Research Note: The influence of frame flexibility on the lateral stability of motorcycles". J.Mech.Eng.Sci. 16 No.2, p.117, 1974.
8. I. Flügge-Lotz, "Discontinuous automatic control". New Jersey Princeton University Press, 1953.
9. J. André & P. Seibert, "Über stuckweise lineare Differential-gleichungen, die bei Regelungsproblem auftreten, I & II". Arch.Math. 7 p.148, 1956
10. B.D.O. Anderson & J.B. Moore, "Linear optimal control". Prentice-Hall, Ch.6 p.99, 1971.
11. A. Gelb & W. van der Velde, "Multiple-input describing functions and non-linear system design". McGraw-Hill, 1968.
12. J.G. Truxall, "Automatic feedback control system synthesis". McGraw-Hill, 1955.

13. R.J. Kochenburger, "A frequency response method of analysing and synthesising contactor servomechanisms". Trans.Amer.Inst.Elect.Engrs. 69 Pt.II, p.270, 1950.

14. Ya. Z. Tsypkin, "Theory of relay systems in automatic control". Moscow, 1958.

15. J.C. Gille, M.J. Pélegrin & P. Decaulne, "Feedback control systems". McGraw-Hill, 1959.